

First Estimations of Cosmological Parameters from BOOMERANG

A.E. Lange,¹ P.A.R. Ade,² J.J. Bock,³ J.R. Bond,⁴ J. Borrill,⁵ A. Boscaleri,⁶ K. Coble,⁷ B.P. Crill,¹ P. de Bernardis,⁸ P. Farese,⁷ P. Ferreira,^{9,10} K. Ganga,^{11,1} M. Giacometti,⁸ E. Hivon,¹ V.V. Hristov,¹ A. Iacoangeli,⁸ A.H. Jaffe,¹² L. Martinis,¹³ S. Masi,⁸ P.D. Mauskopf,¹⁴ A. Melchiorri,⁸ T. Montroy,⁷ C.B. Netterfield,¹⁵ E. Pascale,⁶ F. Piacentini,⁸ D. Pogosyan,⁴ S. Prunet,⁴ S. Rao,¹⁶ G. Romeo,¹⁶ J.E. Ruhl,⁷ F. Scaramuzzi,¹³ and D. Sforna⁸

¹*California Institute of Technology, Pasadena, CA, USA*

²*Queen Mary and Westfield College, London, UK*

³*Jet Propulsion Laboratory, Pasadena, CA, USA*

⁴*Canadian Institute for Theoretical Astrophysics, University of Toronto, Canada*
⁵*National Energy Research Scientific Computing Center, LBNL, Berkeley, CA, USA*

⁶*IROE-CNR, Firenze, Italy*

⁷*Dept. of Physics, Univ. of California, Santa Barbara, CA, USA*

⁸*Dipartimento di Fisica, Universita' La Sapienza, Roma, Italy*

⁹*Astrophysics, University of Oxford, NAPL, Keble Road, OX2 6HT, UK*

¹⁰*Dept. de Physique Theorique, Universite de Geneve, Switzerland*

¹¹*Physique Corpusculaire et Cosmologie, College de France,
11 place Marcelin Berthelot, 75231 Paris Cedex 05, France*

¹²*Center for Particle Astrophysics, University of California, Berkeley, CA, USA*

¹³*ENEA Centro Ricerche di Frascati, Via E. Fermi 45, 00044 Frascati, Italy*

¹⁴*Dept. of Physics and Astronomy, University of Massachusetts, Amherst, MA, USA*

¹⁵*Depts. of Physics and Astronomy, University of Toronto, Canada*

¹⁶*Istituto Nazionale di Geofisica, Roma, Italy*

The anisotropy of the cosmic microwave background radiation contains information about the contents and history of the universe. We report new limits on cosmological parameters derived from the angular power spectrum measured in the Antarctic flight of the BOOMERANG experiment within the framework of inflation-motivated adiabatic cold dark matter models. Using a weak prior probability on the Hubble expansion parameter h we find the curvature is close to flat and the primordial fluctuation spectrum is nearly scale invariant, in agreement with the basic inflation paradigm. We find that the data prefer a baryon density $\Omega_b h^2$ above, though similar to, the estimates from light element abundances and big bang nucleosynthesis. When combined with large scale structure observations, the BOOMERANG data provide evidence for both dark matter and dark energy contributions to the total energy density Ω_{tot} .

The angular power spectrum \mathcal{C}_ℓ of temperature anisotropy in the cosmic microwave background (CMB) is a powerful probe of the content and nature of the universe. The DMR instrument on the COBE satellite measured \mathcal{C}_ℓ for multipoles $\ell \lesssim 20$, corresponding to angular scales larger than $\sim 5^\circ$ [1]. Significant experimental effort by many groups focusing on smaller angular scales, when combined [2, 3, 4], led to the \mathcal{C}_ℓ estimates in the ℓ bands marked with closed circles in Figure 1, which indicate a peak at $\ell \sim 200$. It has long been recognized that if \mathcal{C}_ℓ can be determined with high precision over these angular scales, parameters such as the total energy density and baryon content of the universe, and the shape of the primordial power spectrum of density fluctuations, could be accurately measured [5]. The most recently published BOOMERANG angular power spectrum shown in Figure 1 represents a qualitative step towards such high precision [7] (hereafter, B98).

The data define a strong peak at $\ell \sim 200$. The steep drop in power from $\ell \sim 200$ to $\ell \sim 400$ is consistent with the structure expected from acoustic oscillations in adiabatic cold dark matter (CDM) models of the universe, but is not consistent with locations and widths of peaks expected in the simplest cosmic string, global topological defect, and isocurvature perturbation models [8]. The

data at higher ℓ also show strong detections which limit the height of a second peak, but are consistent with the height expected in many CDM models.

In this paper, we concentrate on determining a set of 7 cosmological parameters that characterize a very broad class of CDM models by statistically confronting the theoretical \mathcal{C}_ℓ 's with the B98 and DMR bandpower data. Sample CDM models that fit the data are shown in Figure 1. These are best-fit theoretical models using successively more restrictive “prior probabilities” on the parameters, a theme of this paper. Some of these priors are quite weak and are generally agreed upon by all cosmologists, for example that the Universe is older than 10 Gyr and that the Hubble constant $H_0 = 100 h \text{ km s}^{-1}\text{Mpc}^{-1}$ lies between 45 and 90. Stronger priors rely on specific measurements, e.g., the HST key project determination of H_0 to 10% accuracy [9] and the determination of the cosmological baryon density, $\omega_b \equiv \Omega_b h^2$, to 10% [10].

In [7], we applied a medium set of priors to the B98 power spectrum to constrain a 6 cosmological parameter model and found a 95% confidence limit for Ω_{tot} of $0.88 < \Omega_{tot} < 1.12$. Row P0 of Table I shows the result for our full 7 parameter set with a similar medium prior (here taken to be $h = 0.65 \pm 0.1$, $\omega_b = 0.019 \pm 0.006$, with Gaussian errors for both). As we progress through the

Table, we show the effect of either weakening or strengthening the prior from this starting point.

Two of our parameters are fundamental for describing the physics of the radiative transport of the CMB through the epoch at $z \sim 1100$, when the photons decoupled from the baryons. These are ω_b and the CDM density $\omega_c \equiv \Omega_c h^2$. The acoustic patterns at decoupling are related to the sound-crossing distance at that time, r_s , which is sensitive to these parameters. We fix the density of photons and neutrinos [11], which are other important constituents at this epoch. The observed B98 patterns are also sensitive to the “angular diameter distance” to photon decoupling, mapping the $z \sim 1100$ spatial structure to the angular structure, and, through its dependence on geometry, to Ω_{tot} , the total energy in units of the critical density. When $\Omega_{tot} < 1$ (open models), r_s is mapped to a small angular scale; when $\Omega_{tot} > 1$ (closed models), r_s is mapped to a large angular scale.

This mapping also depends upon the density associated with a cosmological constant, Ω_Λ , and $\Omega_m \equiv (\omega_c + \omega_b)/h^2$. Combinations of Ω_m and Ω_Λ which give the same angular diameter distance will give nearly identical CMB patterns, resulting in a near degeneracy that is broken only at large angular scales where photon transport through time-varying gravitational potentials plays a role. One implication of this is that Ω_Λ cannot be well determined by our data alone, in spite of the high precision of B98. We have paid special attention to such near-degeneracies [12] throughout our analysis.

The universe reionized sometime between photon decoupling and $z \sim 5$. This suppresses \mathcal{C}_ℓ at small scales by a factor $e^{-2\tau_C}$, where τ_C , our fifth parameter, is the optical depth to Thompson scattering from the epoch at which the universe reionized to the present.

Our last two parameters characterize the nature of the fluctuations arising in the early universe, through a power law “tilt” n_s and an overall amplitude factor for the primordial perturbations. The simplest inflation models have a nearly scale invariant spectrum characterized by $n_s \approx 1$. Of course, many more variables, and even functions, may be needed to specify the primordial fluctuations, in particular those describing the possible contribution of gravity waves, whose role we have also tested [13]. For our overall amplitude parameter, we use $\ln \mathcal{C}_{10}$ where \mathcal{C}_{10} is the CMB power in the theoretical spectrum at $\ell = 10$. If we wish to relate the CMB data to large scale structure observations of the Universe (LSS), we use $\ln \sigma_8^2$ as the amplitude parameter, where σ_8^2 is the model power in the density fluctuations on the scale of clusters of galaxies ($8h^{-1}\text{Mpc}$).

Our adopted parameter space is therefore $\{\omega_b, \omega_c, \Omega_{tot}, \Omega_\Lambda, n_s, \tau_C, \ln \mathcal{C}_{10}\}$. The amplitude \mathcal{C}_{10} is a continuous variable, and the rest are discretized for the purpose of constructing the model database we use to compare data and theory. The number of values and coverage are: 15, over $0.1 \leq \Omega_{tot} \leq 1.5$; 14, over $0.0031 \leq \omega_b \leq 0.2$; 10, over $0.03 \leq \omega_c \leq 0.8$; 11, over $0 \leq \Omega_\Lambda \leq 1.1$; 9, over $0 \leq \tau_C \leq 0.5$; 31,

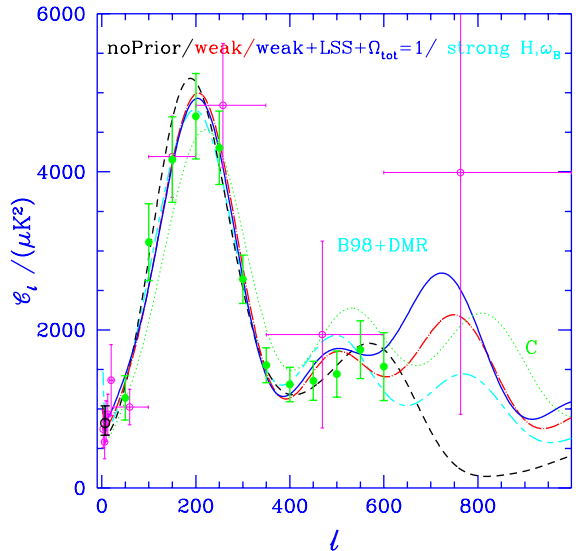


FIG. 1: CMB angular power spectra, $\mathcal{C}_\ell \equiv \ell(\ell + 1)\langle |T_{\ell m}|^2 \rangle/(2\pi)$, where the $T_{\ell m}$ are the multipole moments of the CMB temperature. The open (green) circles show the B98 data. The closed (magenta) circles with horizontal error bars are a radical compression of all the data prior to B98 into optimal bandpowers [2, 3, 4], showing the qualitative improvement provided by B98 except in the $\ell \lesssim 20$ DMR regime. (Note that the B98 and prior CMB points at $\ell = 150$ lie on top of each other.) The smooth curves depict power spectra for several maximum likelihood models with different priors chosen from Table I, with $(\Omega_{tot}, \omega_b, \omega_c, \Omega_\Lambda, n_s, \tau_C)$ as follows: P1, short dashed line, $(1.3, 0.10, 0.80, 0.6, 0.80, 0.025)$; P4, dot-dashed line, $(1.15, 0.03, 0.17, 0.4, 0.925, 0)$; P8, short-long dashed line, $(1.05, 0.02, 0.06, 0.90, 0.825, 0)$; P11, solid line, $(1.0, 0.03, 0.27, 0.60, 0.975, 0)$. These curves are reasonable fits to the B98+COBE data, but differ greatly at $\ell > 600$. For comparison, we plot a $H_0 = 68$, $\Omega_\Lambda = 0.7$ “concordance model” which does not fit (dotted line labelled C), with parameters $(1.0, 0.02, 0.12, 0.70, 1.0, 0)$.

over $0.5 \leq n_s \leq 1.5$. The spacings in each dimension are uneven, designed to concentrate coverage in the regions preferred by the data and yet still map the outlying regions. Fast CMB transport programs [14] were used to construct our \mathcal{C}_ℓ databases. Use was made of the angular-diameter distance degeneracy and ℓ -space compression to reduce the size and computational requirements needed to construct such a database. In the course of this work, we have also explored a number of other parameter space choices; for example a finely gridded one using $\{\Omega_c, \Omega_b, h\}$ in place of $\{\Omega_{tot}, \omega_b, \omega_c\}$. This allowed us to test the influence of discretization and different variable combinations on our results. We find excellent agreement between the results of the different parameterizations.

Parameter estimation is an integral part of the B98 analysis pipeline, which makes statistically well-defined maps and corresponding noise matrices from the time-ordered data, from which we compute a set of maxi-

imum likelihood bandpowers, \mathcal{C}_B . The likelihood curvature matrix $\mathcal{F}_{BB'}$ is calculated to provide error estimates including correlations between bandpowers. The curvature matrix $\mathcal{F}_{BB'}$ and the curvature matrix evaluated at zero signal, $\mathcal{F}_{BB'}^0$, are used in the offset-lognormal approximation [2] to compute likelihood functions $L(x, \vec{y}) = P(\vec{\mathcal{C}}_B | x, \vec{y})$ for each combination of parameters x and \vec{y} in our database. Here x is the value of the parameter we are limiting, \vec{y} specifies the values of the other parameters.

We multiply the likelihood by our chosen priors, and marginalize over the values of the other parameters \vec{y} , including the systematic uncertainties in the beamwidth and calibration of the measurement [15]. This yields the marginalized likelihood distribution

$$\mathcal{L}(x) \equiv P(x | \vec{\mathcal{C}}_B) = \int P_{prior}(x, \vec{y}) L(x, \vec{y}) d\vec{y}. \quad (1)$$

For clear detections, central values and 1σ limits for the explicit database parameters mentioned above are found from the 16%, 50% and 84% integrals of $\mathcal{L}(x)$. When no clear detection exists, these errors can be misleading, so for these cases we shift to likelihood falloffs by $e^{-1/2}$ from the maximum, or variances about the mean of the distribution $\mathcal{L}(x)$. The mean and variance are used to set the limits on other “auxiliary” parameters such as h and Ω_m , which may be nonlinear combinations of the database variables. For good detections the three estimation methods give very good agreement, and yield 2σ errors that are roughly twice the 1σ ones generally reported in this paper.

We have used this method to estimate parameters, using the B98 power spectrum of Figure 1 with the COBE bandpowers determined by [2] and a variety of priors. The results are summarized in Table I; likelihood functions for selected parameters and priors are shown in Figure 2.

In the presence of degenerate and ill-constrained combinations of parameters, as with CMB data, the edges of the data-base form implicit priors. We have constructed our database such that these effective priors are extremely broad. This allows us to probe the dependence of our results on individually imposed priors. The choice of measure on the space is itself a prior; we have used a linear measure in each of our variables [16]. Priors can break parameter degeneracies and result in more stringent limits on the cosmological parameters. Artificially restrictive databases or priors can lead to misleading results; thus, priors should be both well motivated and tested for stability. We therefore regard it as essential that the role of “hidden priors” in any choice for \mathcal{C}_ℓ database construction be clearly articulated.

We now discuss the results of this exercise, in the general order of weakest to strongest applied priors.

Our “entire database” analysis prefers closed models with very high ω_b , as shown in line P1 of Table I and in Figure 2. The low sound speed of these models couples with the closed geometry to fit the peak near $\ell \sim 200$. These models require very high values of h and ω_b , and

have extremely low ages, so we have mapped out this region using a coarse grid. Applying weak priors (lines P2-P4 in Table I) moves the result away from those models, to a regime which is stable upon application of further priors and analysis with smaller databases, as shown in panels 1 (top left) and 4 (bottom left) of Figure 2. Given their gross conflict with multiple other cosmological tests we do not advocate the “entire database” models as representative of the actual universe, and we proceed with prior-limited analyses below.

The analysis with weak priors (P2-P4) finds that the curvature is nearly flat, while favoring slightly closed models. The migration toward $\Omega_{tot} = 1$ as additional priors are applied, as shown in Table I and panel 1 of Figure 2, suggests caution in the overinterpretation of 1σ effects. The baryon density ω_b is also well constrained. While our results are in formal statistical disagreement with the ω_b estimates from light element abundances [10], it is none the less remarkable that our entirely independent method yields a result that is so close. The scalar spectral index n_s is very stable once weak priors are applied, and is near the value expected from inflation. This weak prior analysis does not yield a significant detection of Ω_Λ ; the $\Omega_c h^2$ results in Table I are suggestive of a detection, but are at least in part driven by the weak priors acting on limits of the database [17, 18]. The values of τ_C are in the range of expectation of the models, but there is no clear detection.

In row P4a, we add a “CMB prior”, which is actually a full likelihood analysis of all prior CMB experiments combined with B98 and DMR, including appropriate filter functions, calibration uncertainties, correlations, and noise estimates for use in the offset-lognormal approximation [2]. As would be expected given the errors we compute on the compressed bandpowers of these experiments in Figure 1 *cf.* those for B98, this CMB prior only slightly modifies the B98-derived parameters, with n_s the most notable migration. None the less, as much previous analysis of the prior heterogeneous CMB datasets has shown [19], reasonably strong cosmological conclusions could already be drawn on n_s and Ω_{tot} . Row P4b shows results for the weak prior case of excluding B98, through our machinery. Though n_s and Ω_k have detections consistent with the B98 results, no conclusions can be drawn on ω_b (though the whole database does pick up the high ω_b , Ω_{tot} region.) We note that if $\tau_c \approx 0$ is enforced, most variables remain unmoved, but n_s , which is well-correlated with τ_C , moves closer to unity: for P4, P4a, P4b, we would have $n_s = 0.97, 0.99, 1.04$, respectively, and for P5, P5a, P5b, we would have $n_s = 0.94, 0.96, 0.99$. A prior probability of τ_C based on ideas of early star formation would help to decrease the n_s degree of freedom.

The Ω_{tot} , ω_b , and n_s results are stable to the addition of a prior which imposes two constraints derived from large scale structure (LSS) observations [6]. The first is an estimate of σ_8^2 that requires the theory in question to reproduce the local abundance of clusters of galax-

ies. The second is an estimate of a shape parameter for the density power spectrum derived from observations of galaxy clustering [20]. Adding LSS to the weak h and BBN priors (P5, and panels 2 (top center) and 3 (top right) of Figure 2) breaks a degeneracy, yielding a weak determination of Ω_Λ that is consistent with “cosmic concordance” models. This also occurs when LSS is added to only the prior CMB data (P5b and [6]). The LSS prior also strengthens the statistical significance of the determination of $\Omega_c h^2$. Panel 3 of Figure 2 shows likelihood contours in the $\Omega_k \equiv 1 - \Omega_{tot}$ vs. Ω_Λ plane. Here we have plotted the LSS prior (P5), which begins to localize the contours [21] away from the $\Omega_\Lambda = 0$ axis, toward a region that is consistent with the SN1a results [22].

The use of a strong h prior alone yields results very similar to those for the weak h case. The strong BBN prior, however, shifts many of the results from the weak BBN case. Our data indicate a higher $\Omega_b h^2$ than BBN, and constraining it with the BBN prior shifts the values of several parameters, including $\Omega_b h^2$, Ω_Λ , n_s , and Ω_m . Additional “strong prior” results (P8-P11) are shown in Table I, as an exercise in the power of combining other constraints with CMB data of this quality.

A number of the cosmological parameters are highly correlated, reflecting weak degeneracies in the broad but

restricted ℓ -space range that the B98+DMR data covers [12]. Some of these degeneracies can be broken with data at higher ℓ , as is visually evident in the radically different behavior of the models of Figure 1 beyond $l \sim 600$. To understand the degeneracies within the context of this data, we have explored the structure of the parameter covariance matrix $\langle \Delta y_i \Delta y_j \rangle$, both for the database parameters and the ones derived from them. They add motivation for the specific parameter choices we have made [23]. Parameter eigenmodes [5, 12] of the covariance matrix, found by rotating into principal components, explicitly show the combinations of physical database variables that give orthogonal error bars. A by-product is a rank-ordered set of eigenvalues, which show that for the current B98 data, 3 combinations of the 7 parameters are determined to better than 10% [24].

The B98 power spectrum reported in Figure 1 was calculated from a coarsely pixelized map made by a single channel over a limited region of the B98 sky coverage. By using more of the B98 data and making maps with finer pixelization, we hope to reduce the errors and extend the bandpower estimates to higher ℓ . Such work, and the estimation of the cosmological parameters it implies, is a primary goal of future analyses of BOOMERANG data.

TABLE I: Results of parameter extraction using successively more restrictive priors. The confidence intervals are 1σ , evaluated using methods described in the text. The 2σ errors are approximately double the 1σ values quoted in most cases. The quoted values are reported after marginalizing over all other parameters. Note that these combinations are not, and should not be, the parameters of the “maximum likelihood” best-fit models of Figure 1. The weak h and BBN ($\Omega_b h^2$) priors are tophat functions (uniform priors) and both include an additional age > 10 Gyr prior. The strong priors are Gaussians with the stated 1σ error. P0 is the medium $h + \text{BBN}$ prior used in [7] and described in the text. The LSS priors are combinations of Gaussians and tophats [20]. Rows P4a and P5a show the small effect of including prior CMB data in our B98+DMR analysis; these should be contrasted with P4b and P5b, the case of prior CMB data alone. Columns 1-5 (Ω_{tot} to Ω_Λ) are predominantly driven by the CMB data, except for $\Omega_b h^2$ and Ω_b when the strong BBN prior (P7-P9) is applied. Most of the values in columns 6-10 (τ_c to Age) are influenced by the structure of the parameter space and should not be interpreted as CMB-driven constraints; exceptions are the $\Omega_c h^2$ results when the LSS prior is applied. An equivalent table that includes an inflation-inspired gravity wave induced contribution to the anisotropy [13] yields remarkably similar parameters and errors.

Priors	Ω_{tot}	$\Omega_b h^2$	n_s	Ω_b	Ω_Λ	τ_c	$\Omega_c h^2$	Ω_m	h	Age
P0: Medium $h + \text{BBN}$	$1.06^{0.05}_{0.05}$	$0.030^{0.004}_{0.004}$	$0.99^{0.08}_{0.08}$	$0.07^{0.02}_{0.02}$	$0.39^{0.22}_{0.24}$	$0.22^{0.15}_{0.14}$	$0.27^{0.11}_{0.11}$	$0.68^{0.22}_{0.22}$	$0.64^{0.06}_{0.06}$	$11.9^{1.6}_{1.6}$
P1: Whole Database	$1.30^{0.16}_{0.16}$	$0.102^{0.029}_{0.034}$	$0.87^{0.11}_{0.08}$	$0.10^{0.05}_{0.05}$	$0.54^{0.21}_{0.26}$	$0.22^{0.19}_{0.16}$...	$0.81^{0.33}_{0.33}$	$1.10^{0.38}_{0.38}$	$7.6^{2.8}_{2.8}$
P2: Weak h ($0.45 < h < 0.90$)	$1.15^{0.10}_{0.08}$	$0.035^{0.005}_{0.005}$	$1.04^{0.10}_{0.09}$	$0.11^{0.04}_{0.04}$	< 0.76	$0.20^{0.19}_{0.15}$	$0.23^{0.08}_{0.09}$	$0.83^{0.29}_{0.29}$	$0.58^{0.10}_{0.10}$	$12.8^{2.1}_{2.1}$
P3: Weak BBN ($\Omega_b h^2 < 0.038$)	$1.15^{0.11}_{0.10}$	$0.032^{0.004}_{0.005}$	$0.99^{0.09}_{0.10}$	$0.15^{0.09}_{0.09}$	< 0.80	$0.16^{0.18}_{0.12}$	$0.18^{0.10}_{0.09}$	$0.88^{0.33}_{0.33}$	$0.51^{0.15}_{0.15}$	$15.2^{4.2}_{4.2}$
P4: Weak $h + \text{BBN}$	$1.13^{0.09}_{0.08}$	$0.032^{0.004}_{0.004}$	$1.01^{0.08}_{0.08}$	$0.10^{0.04}_{0.04}$	< 0.78	$0.16^{0.18}_{0.14}$	$0.22^{0.08}_{0.09}$	$0.80^{0.29}_{0.29}$	$0.58^{0.10}_{0.10}$	$13.0^{2.2}_{2.2}$
P4a: Weak & prior CMB	$1.14^{0.09}_{0.09}$	$0.032^{0.003}_{0.003}$	$1.06^{0.08}_{0.08}$	$0.10^{0.04}_{0.04}$	< 0.76	$0.33^{0.12}_{0.14}$	$0.24^{0.08}_{0.08}$	$0.82^{0.27}_{0.27}$	$0.58^{0.10}_{0.10}$	$12.7^{1.7}_{1.7}$
P4b NO B98: Weak & prior CMB	$1.05^{0.16}_{0.10}$	$0.020^{0.011}_{0.014}$	$1.20^{0.11}_{0.14}$	$0.06^{0.04}_{0.04}$	< 0.73	$0.36^{0.10}_{0.14}$	$0.21^{0.09}_{0.08}$	$0.70^{0.28}_{0.28}$	$0.59^{0.11}_{0.11}$	$13.2^{2.9}_{2.0}$
P5: LSS & Weak $h + \text{BBN}$	$1.12^{0.08}_{0.08}$	$0.032^{0.004}_{0.004}$	$0.98^{0.08}_{0.07}$	$0.10^{0.04}_{0.04}$	$0.50^{0.15}_{0.19}$	$0.16^{0.18}_{0.11}$	$0.19^{0.06}_{0.05}$	$0.66^{0.21}_{0.21}$	$0.59^{0.11}_{0.11}$	$13.4^{1.7}_{1.7}$
P5a: LSS & Weak & prior CMB	$1.12^{0.07}_{0.08}$	$0.031^{0.004}_{0.003}$	$1.02^{0.08}_{0.07}$	$0.10^{0.04}_{0.04}$	$0.51^{0.15}_{0.19}$	$0.32^{0.12}_{0.15}$	$0.18^{0.06}_{0.05}$	$0.61^{0.20}_{0.20}$	$0.60^{0.11}_{0.11}$	$13.4^{1.7}_{1.7}$
P5b NO B98: LSS & Weak & CMB	$1.01^{0.08}_{0.08}$	$0.022^{0.010}_{0.013}$	$1.11^{0.12}_{0.11}$	$0.06^{0.04}_{0.04}$	$0.54^{0.17}_{0.21}$	$0.34^{0.11}_{0.14}$	$0.21^{0.09}_{0.08}$	$0.50^{0.19}_{0.19}$	$0.61^{0.12}_{0.12}$	$14.0^{2.0}_{2.0}$
P6: Strong h ($h = 0.71 \pm 0.08$)	$1.09^{0.07}_{0.05}$	$0.036^{0.005}_{0.005}$	$1.04^{0.09}_{0.08}$	$0.08^{0.03}_{0.03}$	< 0.77	$0.20^{0.19}_{0.14}$	$0.26^{0.08}_{0.09}$	$0.70^{0.26}_{0.26}$	$0.67^{0.08}_{0.08}$	$11.6^{1.4}_{1.4}$
P7: Strong BBN ($\Omega_b h^2 = 0.019 \pm 0.002$)	$1.10^{0.04}_{0.05}$	$0.021^{0.003}_{0.002}$	$0.84^{0.08}_{0.07}$	$0.07^{0.02}_{0.02}$	$0.80^{0.07}_{0.28}$	$0.09^{0.12}_{0.07}$	$0.08^{0.06}_{0.03}$	$0.37^{0.20}_{0.20}$	$0.54^{0.10}_{0.10}$	$18.0^{2.8}_{2.8}$
P8: Strong $h + \text{BBN}$	$1.05^{0.04}_{0.03}$	$0.021^{0.003}_{0.002}$	$0.86^{0.07}_{0.07}$	$0.05^{0.02}_{0.02}$	$0.78^{0.11}_{0.25}$	$0.08^{0.11}_{0.06}$	$0.09^{0.08}_{0.03}$	$0.26^{0.18}_{0.18}$	$0.68^{0.09}_{0.09}$	$15.4^{2.2}_{2.2}$
P9: LSS & Strong $h + \text{BBN}$	$1.03^{0.05}_{0.05}$	$0.023^{0.003}_{0.003}$	$0.92^{0.06}_{0.06}$	$0.06^{0.02}_{0.02}$	$0.56^{0.12}_{0.15}$	$0.07^{0.11}_{0.06}$	$0.18^{0.06}_{0.05}$	$0.49^{0.14}_{0.14}$	$0.65^{0.08}_{0.08}$	$13.0^{1.5}_{1.5}$
P10: $\Omega_{tot} = 1$ & Weak $h + \text{BBN}$	1	$0.032^{0.004}_{0.003}$	$1.03^{0.07}_{0.07}$	$0.05^{0.01}_{0.01}$	< 0.64	$0.11^{0.14}_{0.08}$	$0.35^{0.11}_{0.09}$	$0.67^{0.21}_{0.21}$	$0.78^{0.08}_{0.08}$	$9.8^{1.0}_{1.0}$
P11: $\Omega_{tot} = 1$ & LSS & Weak $h + \text{BBN}$	1	$0.031^{0.003}_{0.004}$	$0.99^{0.06}_{0.06}$	$0.05^{0.01}_{0.01}$	$0.55^{0.08}_{0.13}$	$0.09^{0.11}_{0.07}$	$0.26^{0.05}_{0.05}$	$0.47^{0.12}_{0.12}$	$0.80^{0.08}_{0.08}$	$10.5^{0.8}_{0.8}$

Acknowledgements:

The BOOMERANG program has been supported by NASA (NAG5-4081 & NAG5-4455), the NSF Science & Technology Center for Particle Astrophysics (SA1477-22311NM under AST-9120005) and NSF Office of Po-

lar Programs (OPP-9729121) in the USA, Programma Nazionale Ricerche in Antartide, Agenzia Spaziale Italiana and University of Rome La Sapienza in Italy, and by PPARC in UK. We thank Saurabh Jha and Peter Garnavich for supplying the SN1a curves used in Figure 2.

[1] C. Bennett *et al.*, *Astrophys. J.* **464**, L1 (1996).
[2] J. R. Bond, A. H. Jaffe and L. Knox, *Astrophys. J.*, **533**, 19, (2000). The bandpowers used to construct the rad-

ically compressed pre-BOOMERANG-LDB spectrum are listed there, except for the [3] and [4] data which we have also included.

[3] A. D. Miller, *et al.*, *Astrophys. J.* **524**, L1 (1999).

[4] P. Mauskopf, *et al.*, submitted to *Astrophys. J.*, astro-ph/9911444 (1999).

[5] e.g., J. R. Bond, G. Efstathiou and M. Tegmark, *Mon. Not. R. Astron. Soc.* **291**, L33 (1997) and references therein; see also [6] for forecasts of LDB parameter extraction performance.

[6] J.R. Bond and A.H. Jaffe, *Phil. Trans. R. Soc. London* **357**, 57 (1999), astro-ph/9809043.

[7] P. deBernardis *et al.*, *Nature* **404**, 955 (2000).

[8] e.g., B. Allen, *et al.*, *Phys. Rev. Lett.* **79**, 2624 (1997); U. Pen, N. Turok and U. Seljak, *Phys. Rev. D* **58**, 023506 (1998); A. Albrecht, R. A. Battye and J. Robinson, *Phys. Rev. D* **59**, 023508 (1999).

[9] W. L. Freedman, astro-ph/9909076 (1999); J. R. Mould, *et al.*, *Astrophys J.* **529**, 786 (2000).

[10] K. A. Olive, G. Steigman and T. P. Walker, submitted to *Phys. Rep.*, astro-ph/9905320 (1999); D. Tytler, J. M. O'Meara, N. Suzuki and D. Lubin, submitted to *Physica Scripta*, astro-ph/0001318 (2000).

[11] The C_ℓ spectra with massive neutrinos are quite similar to those without, and current data, including B98, will not be able to strongly constrain the value. When the LSS prior is added to the CMB data, however, the combination is quite powerful, e.g., [6].

[12] G. Efstathiou and J. R. Bond, *Mon. Not. R. Astron. Soc.* **304**, 75 (1999).

[13] Gravity waves (GW) can induce CMB anisotropy, and could have a separate tilt, n_t , and an overall amplitude. They have little effect over the range of ℓ 's that B98 is most sensitive to, but could have an important impact on the amplitude relative to COBE. To test the role that GW induced anisotropies would play, we have adopted the model used by [6]: for $n_s < 1$, we set $n_t = n_s - 1$ and for $n_s > 1$, we allow no GW contribution. This presents a fixed alternative, reasonably motivated by inflation, without introducing new parameters. We have found that there is a negligible effect on the parameter determinations in Table I; there is only a very slight migration upward in n_s .

[14] U. Seljak and M. Zaldarriaga, *Astrophys. J.* **469**, 437 (1996), <http://www.sns.ias.edu/~matiasz/CMBFAST/cmbfast.html>; A. Lewis, A. Challinor and A. Lasenby, astro-ph/9911177 (1999).

[15] Apart from the 7 stated database parameters, we have allowed for an estimated 10% uncertainty in the calibration and the beam, which we determine simultaneously with the overall amplitude C_{10} , by relaxing to the maximum likelihood value in these variables. We then determine the Fisher error matrix, assume that the variables are log-normally distributed, and evaluate a correction to the likelihoods appropriate for marginalization over these “intrinsic” variables. Including the marginalization correction makes little difference. We have also marginalized over bins that were used in creating the power spectrum but not in the analysis, since they are correlated.

[16] The choice of measure is not important for strong localized peaks, but can potentially affect limits on poorly constrained variables and on those with complex likelihood functions. One can argue for logarithmic measures in C_{10} (as we have used) and in ω_b and ω_c (which we have not used), and there are certainly philosophical alternatives to linear measures in Ω_{tot} and Ω_Λ . Consider what happens when we turn the “whole database” ω_b likelihood curve of Figure 2 into a probability curve if we adopt a logarithmic rather than linear measure: the anomalous peak at 0.1 drops below the “cosmological peak” at 0.03; once weak priors are adopted, the 0.03 peak is all that is left and it is very stable to changing the measure. Changing measures usually moves peaks a small fraction of a σ , although the amount does depend upon relationships to correlated variables with large errors. The discreteness of our database is also a restriction on how accurately we can localize peaks. For example, our finest gridding in Ω_{tot} is 0.05 from 0.8 to 1.2, hence accurate localization better than half this spacing should not be expected. When projections are made, the available volume of models leads to effective priors as well [17, 18].

[17] The weak prior by itself actually focuses ω_c about 0.22, dropping to either side because of h and age restrictions. Our data do constrain ω_c further, but not enough to claim a CMB determination beyond the prior until the LSS prior is included.

[18] Ω_Λ and Ω_{tot} have a prior probability dropping as Ω_{tot} drops and Ω_Λ rises just because Ω_m is positive. There is a physical effect that also favors the closed models when CMB is added. As ω_b varies, the sound speed lowers, the peak moves to higher ℓ , but can be mapped back to our observed ℓ_{pk} by judiciously choosing an $\Omega_{tot} > 1$. $\Omega_\Lambda > 0$ moves the peak to lower ℓ which $\Omega_{tot} < 1$ can also move back to the observed ℓ_{pk} , but it is a smaller effect. If we had allowed $\Omega_\Lambda < 0$, closed models could have done the same, further favoring $\Omega_{tot} > 1$ because of the volume of models available.

[19] e.g., M. White *et al.*, *Mon. Not. R. Astron. Soc.* **283**, pp107, (1996); K. Ganga *et al.*, *Astrophys. J.* **484**, 7 (1997); C. Lineweaver, *Astrophys. J.* **505**, 69 (1998); ref. [6]; G. Efstathiou *et al.*, *Mon. Not. R. Astron. Soc.* **303**, pp47, (1998); S. Dodelson and L. Knox, *Phys. Rev. Lett.* **84**, 3523 (2000); A. Melchiorri *et al.*, submitted to *Astrophys. J.*, astro-ph/9911445 (1999); M. Tegmark and M. Zaldarriaga, *Astrophys. J.*, in press, astro-ph/0002091 (2000); M. Le Dour *et al.*, submitted to *Astron. and Astrophys.*, astro-ph/0004282 (2000).

[20] The LSS prior is a slight modification of the one used in [6]. $\sigma_8 \Omega_m^{0.56} = 0.55^{+0.02,+0.11}_{-0.02,-0.08}$ is assumed to be distributed as a Gaussian smeared by a tophat distribution, with the first error indicating the 1- σ error on the Gaussian, and the second indicating the extent of the tophat about the mean. The constraint from power spectrum shapes involves a combination of spectrum tilt, $n_s - 1$, and a “scaling shape parameter” $\Gamma \approx \Omega_m h e^{-(\Omega_B(1+\Omega_m^{-1}(2h)^{1/2})-0.06)}$ which is related to the horizon scale when the Universe passed from relativistic to matter dominance: $\Gamma + (n_s - 1)/2 = 0.22^{+0.07,+0.08}_{-0.04,-0.07}$. Both priors were designed to generously encompass the observations, and so are “weak” to “medium” rather than “strong”, in the sense of Table I.

[21] The contours plotted at $\mathcal{L}/\mathcal{L}_{max} = \exp[-\{1, 4, 9\}/2]$ provide only rough indicators of 1, 2, and 3 σ ; less restrictive estimates appropriate to symmetric errors in the two variables are also often plotted [12].

[22] Riess *et al.*, *Astron. J.* **116**, 1009 (1998); S. Perlmutter *et al.*, *Astrophys. J.* **517**, 565 (1999).

[23] Here are some sample correlation coefficients for the weak $h+BBN$ case of Table I: it is relatively small between ω_b

and other database variables but between Ω_B and h it is 90%. Similarly, as is evident from the contour map in Figure 2, Ω_k and Ω_Λ are correlated only at the 35% level, whereas Ω_m and Ω_Λ are correlated at the 97% level. Thus, for CMB work it is advantageous to use Ω_k as a variable rather than Ω_m , and hence this is what we plotted in Figure 2 rather than the more recognizable Ω_m - Ω_Λ plot. ω_c and Ω_Λ have a 76% correlation, not surprising in view of that for Ω_m .

[24] For the P4 case, the best determined eigenmode (to ± 0.03) is a combination of slope, amplitude and Thomp-

son depth; next (to ± 0.04) is predominantly Ω_k , with a judicious negative contribution from Ω_Λ , a combination orthogonal to the angular diameter distance degeneracy; the third eigenmode (to ± 0.08) is mostly ω_b , with a little contribution from all other variables. The next three combinations are determined to ± 0.15 , the worst (± 0.4) combination is one of ω_c and Ω_Λ . Similar coefficients and accuracies hold for other priors, except for distortions in the strong BBN prior case.

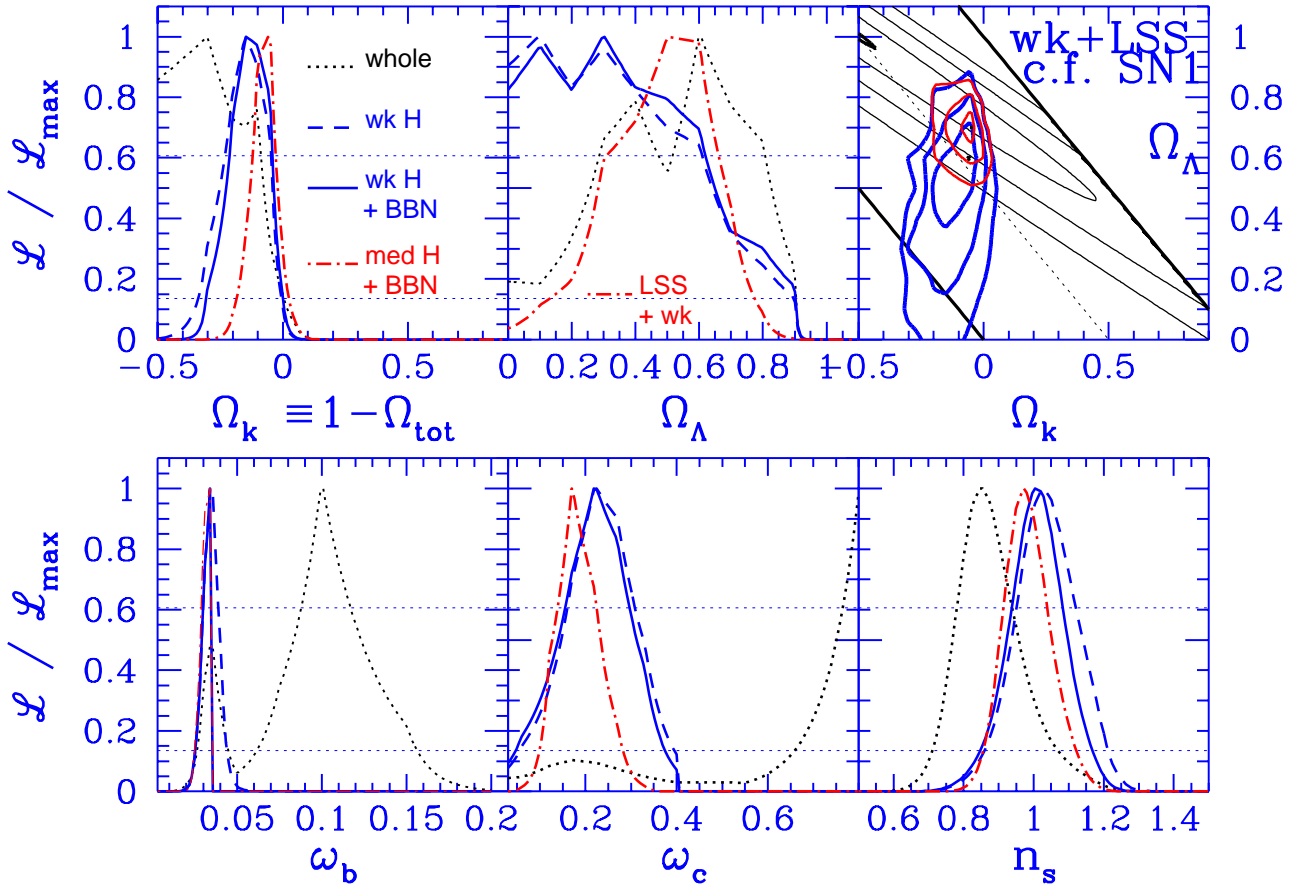


FIG. 2: Likelihood functions for a subset of the priors used in Table I. Panel 1 (top left) shows the likelihood for $\Omega_k \equiv 1 - \Omega_{tot}$; the full-database (P1, dotted line) prefers closed models, but reasonable priors (P2, dashed line; P4, solid line) progressively move toward $\Omega_k = 0$. The medium prior P0 of [7] is dot-dashed. We caution the reader against aggressively interpreting any 2σ effects. Likelihood curves for Ω_Λ are shown in panel 2 (top center). In panels 2 and 4-6, the cases and line types are as in panel 1, except that dot-dashed now denotes the weak+LSS prior, P5. With weak priors applied, no significant limit on Ω_Λ is set (P2, dashed line; P4, solid line in all remaining $\mathcal{L}(x)$ panels). Only by adding the LSS prior is Ω_Λ localized away from zero (P5, dot-dash in all remaining $\mathcal{L}(x)$ panels). Panel 3 (top right) shows the contour plot of Ω_k and Ω_Λ , for which the first two panels are projections to one axis. The bold diagonal lines mark $\Omega_m=1$ and $\Omega_m=0$. The bold (blue) contours are those found with the LSS prior (P5), plotted at 1, 2, and 3σ . SN1a constraints are similarly plotted as the lighter (black) smooth contours, and are consistent with the CMB contours at the 1σ level. When the SN1a prior is applied as well, the result is the light (red) contours, localized near $\Omega_\Lambda \sim 0.7$. Panel 4 (bottom left) shows the contours for ω_b ; the full database analysis results in a bimodal distribution with the higher peak concentrated at very high values. These high ω_b models are eliminated by the application of a weak h prior (P2, dashed). Even the weak BBN prior (P4, solid) clearly overconstrains the data. Panel 5 (bottom center) shows a localization of ω_c for the weak h and BBN prior cases, but this is partially due to the effect of the database structure coupling to the h and age priors. Only the LSS prior (P5, dot-dash) allows the CMB to significantly constrain ω_c . Panel 6 (bottom right) shows good localization and consistency in the n_s determination once any priors are applied. The inflation-motivated $\Omega_{tot}=1$ priors (P10, P11) give very similar curves localized around unity.